

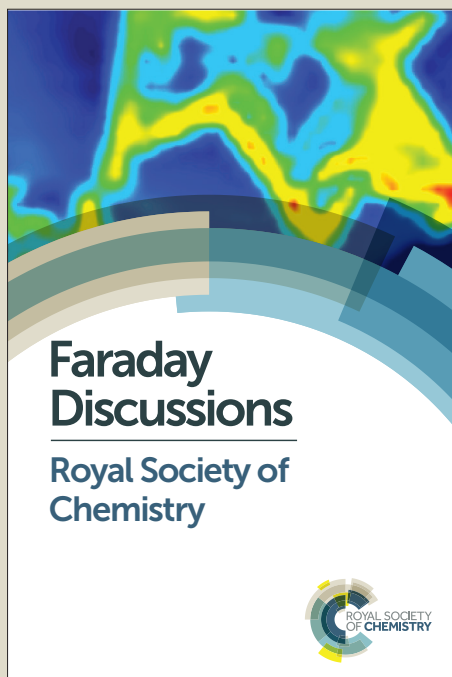
Faraday Discussions

Accepted Manuscript



This manuscript will be presented and discussed at a forthcoming Faraday Discussion meeting. All delegates can contribute to the discussion which will be included in the final volume.

Register now to attend! Full details of all upcoming meetings: <http://rsc.li/fd-upcoming-meetings>



This is an *Accepted Manuscript*, which has been through the Royal Society of Chemistry peer review process and has been accepted for publication.

Accepted Manuscripts are published online shortly after acceptance, before technical editing, formatting and proof reading. Using this free service, authors can make their results available to the community, in citable form, before we publish the edited article. We will replace this *Accepted Manuscript* with the edited and formatted *Advance Article* as soon as it is available.

You can find more information about *Accepted Manuscripts* in the [Information for Authors](#).

Please note that technical editing may introduce minor changes to the text and/or graphics, which may alter content. The journal's standard [Terms & Conditions](#) and the [Ethical guidelines](#) still apply. In no event shall the Royal Society of Chemistry be held responsible for any errors or omissions in this *Accepted Manuscript* or any consequences arising from the use of any information it contains.

1 **Biologically controlled synthesis and assembly of magnetite**
2 **nanoparticles.**

3

4 Mathieu Bennet,^a Luca Bertinetti,^a Robert Neely,^b Andreas Schertel,^c André Körnig,^a Cristina
5 Flors,^d Frank D. Müller,^e Dirk Schüler,^e Stefan Klumpp,^f and Damien Faivre*^a

6

7 ^a*Department of Biomaterials, Max Planck Institute of Colloids and Interfaces, Science Park*
8 *Golm, 14424 Potsdam, Germany*

9 ^b*The University of Birmingham, School of Chemistry, Edgbaston, Birmingham, B15 2TT, UK*

10 ^c*Carl Zeiss Microscopy GmbH, Training, Application and Support Center, Carl-Zeiss-Str. 22,*
11 *73447 Oberkochen, Germany*

12 ^d*Madrid Institute for Advanced Studies in Nanoscience (IMDEA Nanociencia), C/Faraday 9,*
13 *Madrid 28049, Spain*

14 ^e*Universität Bayreuth, Lehrstuhl für Mikrobiologie, Universitätsstraße 30, 95447 Bayreuth,*
15 *Germany*

16 ^f*Department of Theory and Biosystems, Max Planck Institute of Colloids and Interfaces,*
17 *Science Park Golm, 14424 Potsdam, Germany*

18

1 **Abstract**

2 Magnetite nanoparticles have size- and shape-dependant magnetic properties. In addition,
3 assemblies of magnetite nanoparticles forming one-dimensional nanostructures have
4 magnetic properties distinct from zero-dimensional or non-organized materials due to
5 strong uniaxial shape anisotropy. However, assemblies of free-standing magnetic
6 nanoparticles tend to collapse and form closed-ring structures rather than chains in order to
7 minimize their energy. Magnetotactic bacteria, ubiquitous microorganisms, have the
8 capability to mineralize magnetite nanoparticles, the so-called magnetosomes, and to direct
9 their assembly in stable chains *via* biological macromolecules.

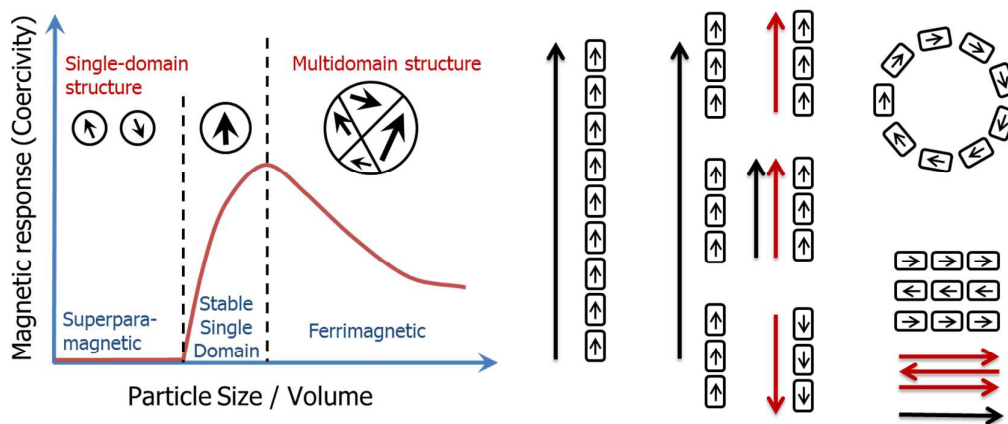
10 In this contribution, the synthesis and the assembly of biological magnetite to obtain
11 functional magnetic dipoles in magnetotactic bacteria is presented, with a focus on the
12 assembly. We present tomographic reconstructions based on cryo-FIB sectioning and SEM
13 imaging of a magnetotactic bacterium to exemplify that the magnetosome chain is indeed a
14 paradigm of a 1D magnetic nanostructure based on the assembly of several individual
15 particles. We show that the biological forces are the major player in the formation of the
16 magnetosome chain. Finally, we demonstrate by super resolution fluorescence microscopy
17 that MamK, a protein of the actin family necessary to form the chain backbone in the
18 bacteria, forms a bundle of filaments that are not only found in the vicinity of the
19 magnetosome chain but widespread within the cytoplasm, illustrating the dynamic
20 localization of the protein within the cells. The very simple microorganisms have thus much
21 to teach in the way to control the design of functional 1D magnetic nanoassembly.

22

1. Introduction

One of the central principles of nanoscience is that the physical properties of nanoparticles are size-dependent. Recent attention in the field has focussed on the assembly of nanoparticles, since new physical properties can emerge as a result of this organization¹. However, whilst many chemical approaches have been developed to control a nanoparticle's dimension or morphology, methods to control their organization have remained scarce².

The iron oxide magnetite (Fe_3O_4) represents the archetype of a nanoparticle as described above. Magnetic properties are indeed size dependent in the nm size-range (Figure 1), with particles smaller than about 30 nm being superparamagnetic (SP, no permanent magnetic signal at room temperature in the absence of an external field), particles larger than 30 nm but smaller than 100 nm being stable single domain (SSD, one domain, remanent magnetization), and particles larger than 100 nm being multidomain (MD, more than one domain, remanent but reduced volume magnetization when compared to SSD)^{3,4}. In addition, the magnetic properties are affected by the morphology of the nanoparticles⁵, their oxidation state⁶, and by their organization^{7,8}.



18

19 Figure 1: scheme of the magnetic properties of individual magnetite nanoparticles (left) and their
 20 assembly (right). Magnetotactic bacteria are able to form magnetosomes of dimensions maximizing

1 their magnetic properties (stable single domain) in a chain organization, which also maximizes their
2 potential of being used as a compass by the cell.

3

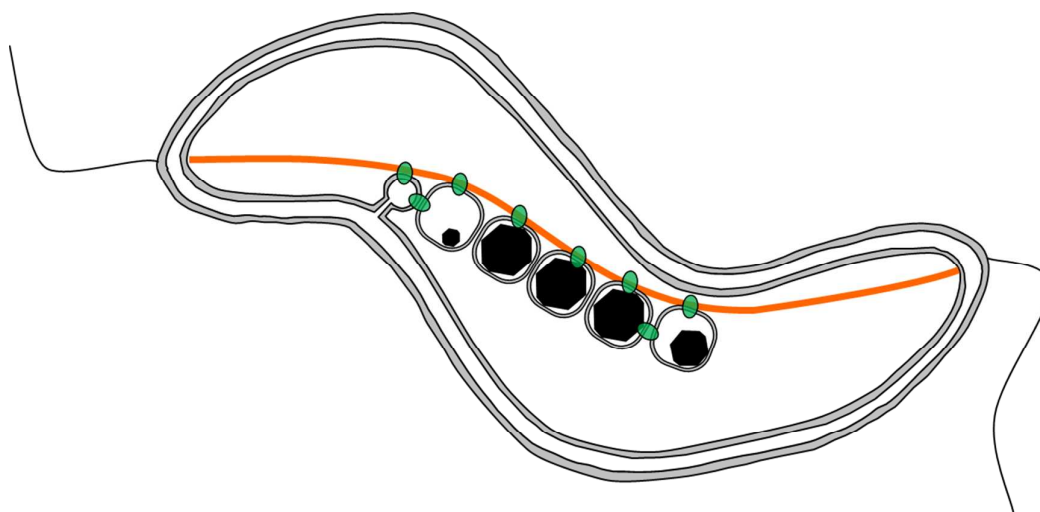
4 Magnetotactic bacteria are ideal candidates to study the synthesis and organization of
5 magnetite nanoparticles. These microorganisms indeed synthesize magnetic nanoparticles
6 called magnetosomes that are membrane-enclosed crystals made of magnetite or greigite
7 (Fe_3S_4 , the iron sulphide equivalent to magnetite)⁹. These nanoparticles are aligned in chain
8 to form a single magnetic dipole strong enough to possibly passively orient the cell along the
9 Earth magnetic field lines, to help the organisms finding their preferred habitat^{10, 11}. The
10 chain is a hierarchically-structured materials made by the assembly of nanoparticles for
11 which the mineralogy¹², the dimension¹³⁻¹⁸, and the crystal orientation¹⁹ is the results of an
12 interplay between physical processes²⁰⁻²³, mostly based on magnetic interactions, and
13 biological control exerted by the bacteria based on its genetic programme²⁴⁻³⁰. In particular,
14 2 proteins have been highlighted for the role they play in the magnetosome chain formation
15 (Figure 2): MamJ, which is only found in magnetospirilla, has been described as the
16 magnetosome connector, which enables the binding of the magnetosome particles to the
17 magnetosome filament, likely made from polymeric subunits of MamK. The *mamK* gene,
18 which is found in the genome of all sequenced magnetotactic bacteria, is a member of the
19 actin family and involved in the building of a backbone to which the magnetosome can
20 attach. The MamK protein forms long bundles of filaments *in vitro*³¹⁻³⁴. *In vivo*, the cells also
21 form long filamentous structures that span along the long axis of the cells from cell pole to
22 cell pole as shown by cryo-electron tomography²⁵⁻²⁷. Tagging MamK with fluorescent
23 markers and studying the localization of the protein by fluorescence microscopy has shown
24 that MamK is at least involved in the building of the filamentous structure *in vivo*^{24, 25}.

25 However, the exact distribution of MamK *in vivo* could not be fully clarified since only a very
26 limited amount of samples have been analysed by cryo-electron tomography where in

1 addition the nature of the filament cannot be granted, and since images obtained by optical
2 fluorescence microscopy do not exhibit a resolution that is sufficient to study this point.
3 MamJ and MamK were shown to interact *in vivo*^{28, 29} and the connection between MamJ and
4 MamK is mechanically extremely stable³⁵. The exact nature of the MamJ-MamK interaction
5 has not yet been elucidated. Evidence for direct interaction of MamJ and MamK comes from
6 two-hybrid assays as well as FRET-experiments^{28, 29}. In addition, mutants in either *mamK* or
7 *mamJ* have no magnetite crystallization defect but display severe magnetosome alignment
8 perturbations. For example, deletion of the *mamJ* gene abolishes formation of a
9 magnetosome chain completely and clusters of magnetosomes are observed within the
10 cells^{27, 28} whereas *mamK* is essential to form a coherent and properly positioned chain in
11 MSR-1 suggesting that both proteins act in the same cellular process of magnetosome
12 positioning²⁵. In addition, in the related organism *Magnetospirillum magnetotacticum* AMB-
13 1, the protein filaments formed by MamK subunits have been shown to be dynamic, and this
14 dynamics depends on MamJ^{24, 31}. Mutants with non-dynamic filaments are impaired in
15 magnetosome chain formation as well. Together, these observations suggest a model in
16 which MamK forms a filament that spans the long axis of the bacterial cell. MamJ anchors
17 the magnetosomes to this filament and may regulate MamK dynamics, which is needed for
18 formation of a coherent magnetosome chain and its proper positioning within the cell.

19

20



1

2 Figure 2: Scheme of a magnetosome chain in a magnetotactic bacterium. The 2 main molecular
3 players are depicted as follows: in orange, MamK forms a filament spanning from one cell pole to the
4 other. In green, MamJ attaches the magnetosome to the filament. However, the clear localization of
5 both proteins is not clear.

6

7 In this communication, we therefore characterize the magnetosome chain by cryo-focused
8 ion beam (cryo-FIB) slicing and scanning electron microscopy (SEM) imaging and confirm the
9 high degree of alignment typically observed for magnetosomes synthesized by the wild-type
10 cells of *Magnetospirillum gryphiswaldense* MSR-1. In addition, we show by super-resolution
11 optical microscopy that MamK filaments are widely dispersed within the cytoplasm of the
12 cell and therefore their localization is not limited to the magnetosome chain as shown so far.

13

14 2. Materials and Methods

15 a. Cryo-FIB imaging and image reconstruction

16 *Sample preparation*

17 Magnetotactic bacteria (*Magnetospirillum gryphiswaldense*) were high pressure frozen using
18 a Leica HPM100. The samples were mounted on a cryo sample holder in the preparation box
19 of the VCT100 shuttle system (Leica Microsystems, Vienna, Austria) at liquid nitrogen
20 temperature. By using the VCT100 shuttle, the sample holder was transferred to the SCD500

1 sputter coater (Leica Micro- systems, Vienna, Austria) at -154 °C cryo-stage temperature and
2 4.10^{-6} mbar chamber pressure. The sample was sputter-coated with a 6 nm platinum layer at
3 0.06 nm s^{-1} . During sputter coating an argon pressure of 2.10^{-2} mbar was used. After coating,
4 the sample was transferred to the Auriga60 CrossbeamR system (Carl Zeiss Microscopy
5 GmbH, Oberkochen, Germany), using the VCT100 shuttle at a cryo-stage temperature of -
6 154°C.

7

8 *Microscopy*

9 A coarse incision was milled directly into the surface of the high pressure frozen sample
10 using the 30 kV : 16 nA FIB probe current in order to achieve a viewing channel for the SEM
11 imaging. A window of about 50 μm in width was fine polished using the 30 kV: 600 pA FIB
12 probe current. For acquisition of the data cube, a block face of about 50 μm width using the
13 600 pA FIB probe current and a slice thickness of 15 nm was defined. The data cube was
14 acquired in a fully automated process. The FIB milling procedure was paused after each slice
15 and the region of interest (ROI) on the block face was imaged using the 7.5 μm aperture in
16 normal mode at 2.33 kV acceleration voltage. Images were acquired with both the in-lens
17 and the back scattered electron (BSE) detectors. The lateral image pixel size was 7.5 nm
18 resulting in images cover- ing 7.72 μm width and 5.79 μm height. Line averaging (N = 256)
19 and a scan speed of 100 ns dwell time were chosen for noise reduction. The cycle time for
20 recording an individual image was 25.2 s. The milling time for removing each slice was 35.8 s.
21 Accordingly, an image was recorded in about a minute. The final image series consisted of 40
22 individual slices resulting in a volume of $7.72 * 5.79 * 0.6 \mu\text{m}^3$.

23

24 *Image analyses*

25 The obtained image sequences obtained using both the in-lens and the BSE detectors were
26 aligned and segmented using the pixel classification workflow of the Ilastik software³⁶. The

1 segmented stacks were imported into Drishti software to generate the 3D visualization. The
2 magnetic particles were rendered using the BSE detector stacks, while the cellular
3 membrane was rendered using the in-lens stack.

4

5 **b. Microscopy**

6 *Sample preparation*

7 *M. gryphiswaldense* cells of strain MSR-1 expressing mCherry-MamK were grown overnight
8 to OD 0.2. One mL of the culture was washed by successive centrifugation for 10 min at 5
9 krpm and resuspension in PBS buffers. The final centrifugation was followed by a
10 resuspension in 40 μ L of low melt agarose at 35 °C. 15 μ L of the agar suspension was
11 sandwiched between a microscope slide and a coverslip placed between magnets and the
12 sample was cooled for 10 min at 5°C. This sample preparation ensured the alignment of the
13 bacteria along the sample plane and allowed observation of live bacteria. For confocal
14 fluorescence microscopy, the bacterial membrane was stained using FM 143 following
15 supplier's recommendation for preparation.

16

17 *Confocal fluorescence microscopy*

18 Conventional fluorescence images were recorded using 488 nm and 561 nm laser line on a
19 confocal microscope (SP5, Leica).

20

21 *Super-resolution fluorescence microscopy*

22 Photoactivated Localisation Microscopy (PALM) is a super-resolution microscopy technique
23 that allows improving an order of magnitude the spatial resolution of standard fluorescence
24 microscopy³⁷. PALM is based on the single molecule detection and localization of
25 photoswitchable fluorophores. By separating the emission of the fluorophores in time, it is
26 possible to individually fit a Gaussian curve to localize with nm precision the molecules in a

1 sample. A map of molecular coordinates of the fluorophores in the sample can be
2 reconstructed with a precision of a few tens of nm. While for a typical PALM experiment a
3 cell needs to be labeled with a photoswitchable fluorescent protein, it is also possible to use
4 the photoblinking of some standard fluorescent proteins such as mCherry in a PALM-like
5 experiment.
6 PALM was carried out on an Olympus IX-83 microscope equipped with a 405 nm, 488 nm,
7 561 nm and 647 nm diode lasers and an oil immersion objective (Olympus OI 150x; NA1.45).
8 Lasers are fiber coupled to the microscope and reflected to the sample using a quad band
9 (405/488/561/635) dichroic filter. Emission was collected via a quad band (25 nm band pass
10 446/523/600/677) emission filter using a Hamamatsu Image-EM EM-CCD camera. Excitation
11 of mCherry is achieved using the 561 nm line. In order to collect sufficient blinking events,
12 sequences of 2000 images were recorded for each mapped area. Super-resolution images
13 were generated using the Localizer plugin³⁸ for Igor Pro (Wavemetrics).

14

15 **3. Results and Discussion**

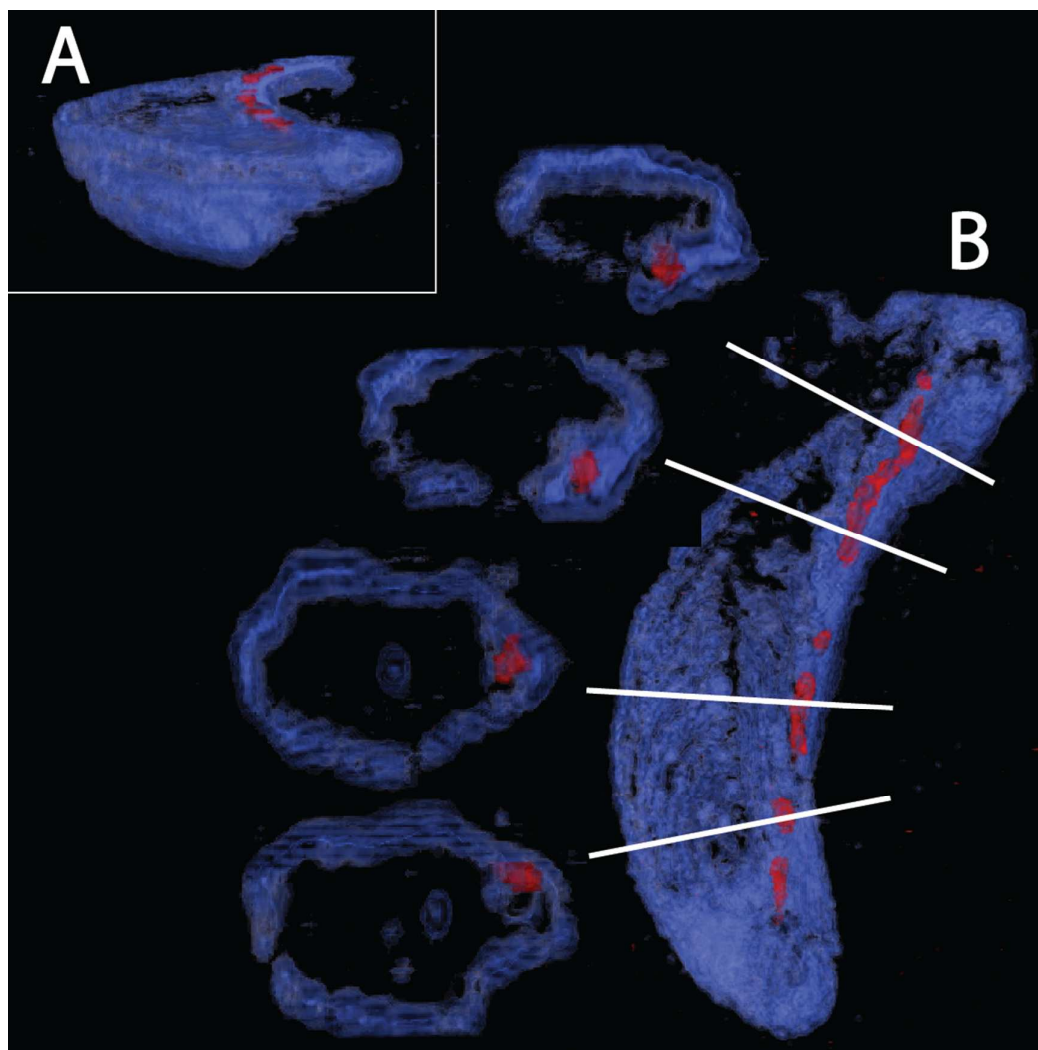
16 **a. The magnetosome chain: paradigm of a 1D magnetic** 17 **nanostucture?**

18 The magnetotactic bacteria and their magnetosome chains are typically imaged using
19 transmission electron microscopy (TEM). In TEM, the bacteria are typically prepared in such
20 a way that they are dried on the surface of a Carbone-film coated grid and the imaging is the
21 result of the projection of the object on a surface. Therefore, several artefacts can originate
22 from the procedure. First, the bacteria, mostly made of organic matter, can be deformed
23 due to drying, thereby possibly deforming the intracellular chain too. In addition, it is not
24 clear how the chain is positioned with respect to the cell envelope since magnetospirilla are
25 helicoidally-shaped. Cryo-electron tomography (CET) has emerged as a powerful technique

1 to avoid the artefacts listed above. In particular, the technique allowed the discovery of the
2 magnetosome filament^{26, 27}. However, several technical difficulties including the so-called
3 missing wedges, angles hardly accessible for imaging due to constraints in the electron
4 microscope column as well as contrast differences between the strongly contrasting
5 magnetite nanoparticles and the poorly contrasting bacterial membrane associated with
6 reconstruction problems make the technique still restrained to few laboratories in the
7 world.

8 Here, we present the first images based on cryo-FIB sectioning of cryogenic fixed
9 magnetotactic bacteria MSR-1 cells imaged by SEM (Figure 3, Supplementary video 1). The
10 3D rendering of a cross section of the cell with the top part being “deleted” by a clipping
11 plane shows that the magnetosomes (particles in red) follow the inner curvature of the cell
12 (cell membrane in blue), resulting in a slightly bent chain (Figure 3A). Magnetosomes, in
13 addition, seem to be present always in close proximity of the membrane (Figure 3B).
14 Magnetosome invaginations were originally shown to be present in AMB-1²⁶ and later in
15 MSR-1, but in the later, it is not clear if this invagination phase is transient or permanent³⁹.
16 The fact that both strains are helicoidally-shaped makes the positioning of the chain along
17 the membrane a very difficult 3D problem: the chain would have to be positioned as the axis
18 of a screw would be with the membrane always being in contact around it. In addition, if the
19 magnetosomes are continuously attached to the inner membrane, the role of the
20 magnetosome filament as a mechanical stabilizer of the chain can be questioned.

21



1

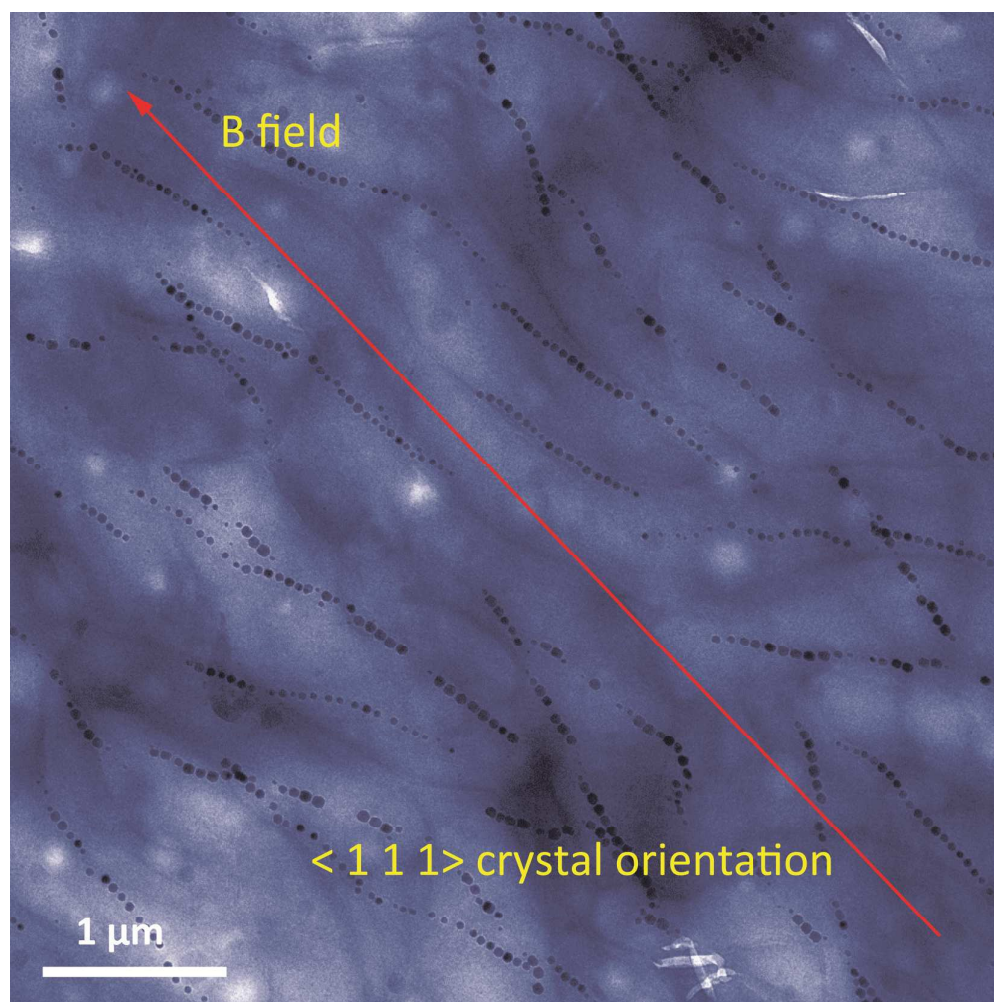
2 Figure 3: 3D rendering of cryo-FIB sectioning and SEM imaging. The cell diameter is typically 500 nm t
3 get an idea about characteristics length scales. A scale bar is not depicted here since the images are
4 snapshots from a 3D rendering with perspective where therefore a pixel size can change as a function
5 of the position on the image.

6

7 **b. Assembly of magnetosomes**

8 As explained above, the magnetosome chain is hierarchically structured. It is formed as the
9 result of the assembly of the individual magnetosomes. In the chain, all the magnetosomes
10 are aligned along the same crystallographic axis, which corresponds to the easy axis of
11 magnetization (Figure 4)¹⁹.

12



1

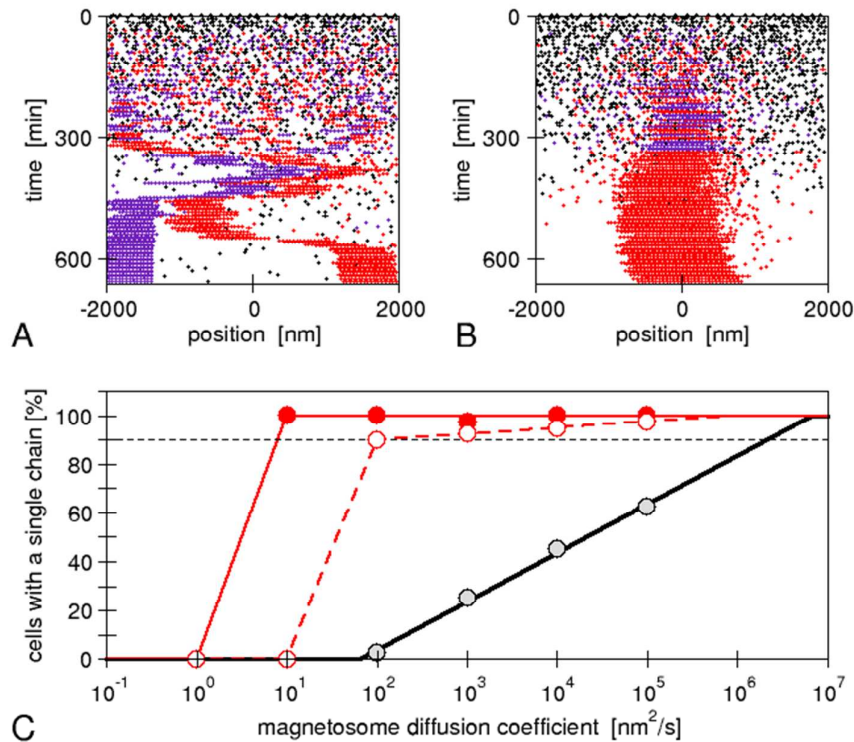
2 Figure 4: false colour transmission electron microscopy image of aligned magnetotactic bacteria. The
3 bacteria are aligned on the TEM grid by the application of a strong external magnetic field. For
4 *Magnetospirillum gryphiswaldense*, the magnetosome crystals are oriented along the $\langle 1 1 1 \rangle$
5 crystallographic direction as depicted on the image. This corresponds to the easy axis of
6 magnetization for isotropic magnetite nanoparticles¹⁹.

7

8 The assembly is performed by the interactions between physical and biological forces. We
9 recently introduced a model to theoretically study the interplay of these forces²². We
10 created "*in silico* mutants" defective not in individual genes, but in entire physical processes,
11 for example, mutants lacking magnetic interactions. Using the model, we have shown that a
12 purely physical process, i.e. the diffusion of the magnetosomes "biased" by their magnetic
13 interactions, does not reliably result in a chain pattern, rather two or even more short chains
14 are observed, typically with different magnetic polarization (Figure 5), a behaviour later

1 observed in another bacterial strain experimentally⁴⁰. Therefore, we concluded that a
2 mechanism of active transport of magnetosomes to the cell centre is required for reliable
3 chain formation. The driving force of such active transport needs to exceed a threshold,
4 which we showed to be easily accessible for a cytoskeletal machinery such as those possibly
5 expected for *mamK*²². Thus, specific biological forces play a critical role in the magnetosome
6 chain assembly. We note however that directed transport might not be absolutely required
7 for chain assembly, but appears to be necessary for the reliable chain assembly in bacterial
8 cells. Indeed, in our simulations, we varied the mobility of the magnetosomes over a wide
9 range (with the mobility of large proteins in bacterial cytoplasm as an upper limit) and
10 observed that chain formation becomes more robust with increasing mobility. By
11 extrapolating our simulation results (Figure 5), we can predict that a diffusion coefficient of 2
12 $\mu\text{m}^2 \text{s}^{-1}$ would be needed for reliable formation of a single chain (in more than 90% of the
13 cells as observed experimentally⁴⁰). Such a high diffusion coefficient might be achieved in an
14 aqueous solution, but is highly unlikely in cytoplasm, where large proteins (with radius 2-5
15 nm) have diffusion coefficients comparable to this value ($1 - 10 \mu\text{m}^2 \text{s}^{-1}$ in bacterial
16 cytoplasm^{41, 42}). Due to the strong size-dependence of diffusion in cytoplasm⁴², diffusion of
17 magnetosomes should be considerably slower, even more so if the magnetosomes are
18 indeed attached to the inner membrane as invaginations. Thus, in a cell, such rapid diffusion
19 could only be achieved through active processes that enhance diffusion through active
20 (energy-dependent) but random motion (“active diffusion”), a mechanisms known for
21 cytoskeletal transport⁴³. This observation indicates that an important constraint/limitation to
22 chain assembly in the cell is the low mobility of large objects such as magnetosomes in the
23 cytoplasm. While active diffusion provides a possible explanation for chain assembly in the
24 cells, there is no direct evidence for such motion. Moreover directed active transport
25 provides the additional benefit of functioning as a mechanism for localizing the chain in the
26 cell centre and for controlled repositioning of the chain after cell division⁴⁴. In either case,

1 the active processes are likely based on the magnetosome filament, which possibly acts as a
 2 polymerization or depolymerization motor.
 3



4
 5 Figure 5: Simulations of *de novo* magnetosome chain formation with and without active transport of
 6 magnetosomes: Simulation trajectories for diffusing magnetosomes (A) and magnetosomes that are
 7 actively transported toward the centre of the cell (B). In both cases, open black circles show empty
 8 magnetosome vesicles, red and violet circles show magnetosomes containing a crystal with negative
 9 and positive orientation of the magnetic moment, respectively. The simulations were done with the
 10 same set of parameters as in ²² and a magnetosome mobility characterized by a diffusion coefficient
 11 of $10^4 \text{ nm}^2 \text{ s}^{-1}$ and an active driving force $F_{\text{act}} = 0.01 \text{ pN}$ (in B). (C) Fraction of simulations that result in
 12 a cell with a single chain as function of the magnetosome mobility (diffusion coefficient). A gradual
 13 increase is obtained for the case of diffusive motion (black circles), while threshold behaviour is seen
 14 for active transport (with $F_{\text{act}} = 0.1$ and 0.01 pN for the solid red and open red circles, respectively).
 15 The lines extrapolate these simulation data (from ²²) to a larger range of mobilities.

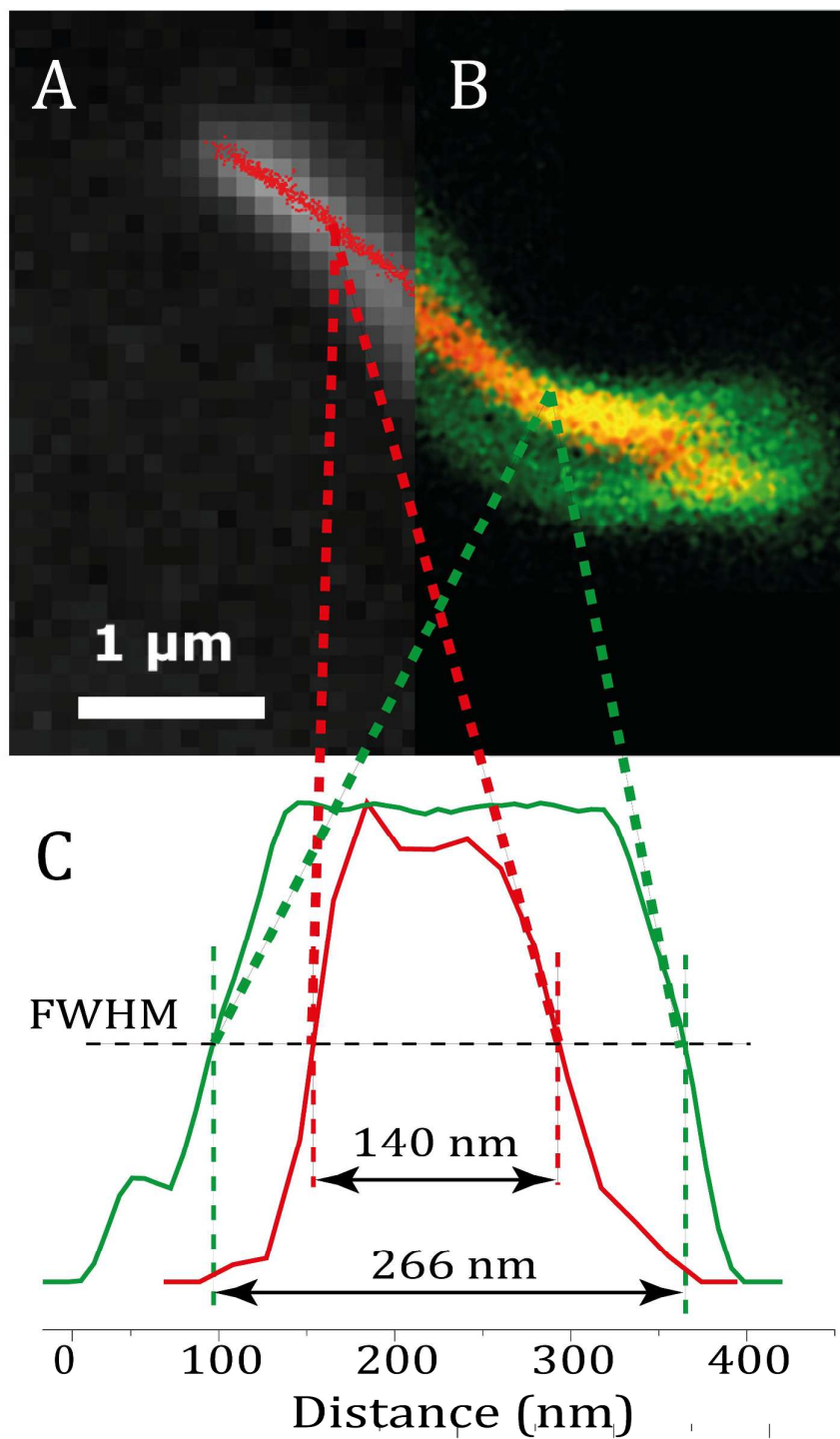
16

17 We have therefore studied the role of biological determinants in more details here. One of
 18 the functions of protein networks *in vivo* is to provide cells with mechanical properties. For
 19 instance, actin is a protein that forms filaments in eukaryotic cells and is used for tasks

1 requiring mechanical forces such as cell motility, maintenance of cell shape and organelles
2 organisation⁴⁵. Because such filaments are too thin to provide contrast by light absorption
3 using regular optical microscopy, researchers image them *in vivo* using fluorescence
4 microscopy and a fluorescence marker. The markers allow detecting the presence and
5 mapping the network of the stained proteins with a maximum resolution given by the
6 diffraction limit theorem, ca. 250 nm in a typical experiment. In some instances, this
7 resolution is not sufficient to gain insight into the protein network properties. As mention
8 above, 2 particular proteins MamJ and MamK have been studied so far, specifically in the
9 magnetospirilla *Magnetospirillum magneticum* and *Magnetospirillum gryphiswaldense*. It
10 has remained unclear if the phenotype observed for the deletion strains i.e. the
11 “observable” characteristics differentiating the mutant from the unmodified “wild-type”
12 cells is directly due to the non-expression of this particular gene and of the resulting non-
13 expression of the associated protein or if this results from an indirect role associated with
14 the process where e.g. other protein expression levels are modified as well. For example, in
15 AMB-1, the roles of *mamJ* and *limJ* are redundant, showing that potentially in the absence of
16 the one, the other gene present in the machinery of the cell, is capable of taking over and
17 therefore also potentially blurring the role played by a giving gene in the organism²⁴. The
18 same redundancy has been observed for *mamK* with the presence of another gene, *mamK*-
19 *like*, that is indeed capable of forming filaments in the *mamK* deletion mutant in AMB-1
20 cells³².

21 Figure 6 shows an image of an mCherry-MamK filament *in vivo* recorded using confocal
22 fluorescence microscopy (Figure 6b) in comparison with a super-resolution image (Figure
23 6a). As can be observed on the extracted profiles (Figure 6c), the extent to which the
24 filament can be located in the cell in the confocal image is limited by the diffraction limit of
25 the optical system, which is slightly better than half the width of the bacterium. In the super-
26 resolution image, each red dot corresponds to the calculated position of an mCherry

1 molecule which has undergone a blinking event. The standard deviation in the determined
2 position of each of these molecules was calculated to be an average of 22 nm across all
3 localized emitters. In contrast, the full-width at half maximum intensity of the filament, shown
4 in Figure 6, is 140 ± 32 nm, much larger than our localization precision, clearly indicating the
5 presence of filaments comprised of supramolecular bundles of proteins in these organisms.



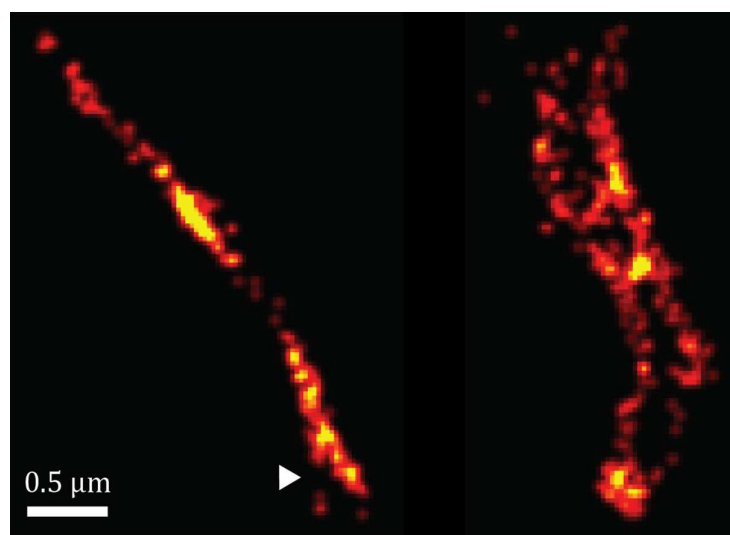
1

2 Figure 6: (a): Super-resolution image of MamK-mCherry filaments (red dots) in a living bacterium; (b)
 3 an equivalent confocal fluorescence image of MamK-mCherry filaments (yellow signal) in a living
 4 bacterium the membrane of which is dyed using FM-143 (green signal). (c): Profile of the fluorescence
 5 signal of mCherry extracted from the super-resolution image (red) and from the confocal image
 6 (green).

7

1 Furthermore, as shown in Figure 7 the spatial distribution of MamK in MSR-1 does not
2 typically correspond to the expected pattern of a single filamentous structure extending
3 from pole to pole of the cell. Indeed, some bacteria exhibit branching of the MamK filament
4 or a heterogeneous (clustered) distribution of the MamK-mCherry construct across the cell.
5 This observation made us revisit our confocal imaging data in more detail, and we indeed
6 find that a majority of bacteria exhibit clustered MamK (Figure 8).

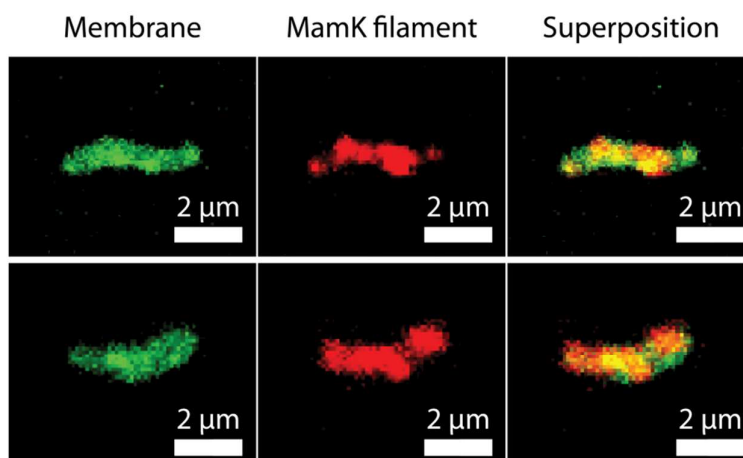
7



8

9 Figure 7: Super-resolution images of the MamK filament *in vivo* showing branching (white triangle).

10



11

12 Figure 8: Confocal fluorescence images of MSR1 MamK_mCherry stained with a membrane dye (FM-
13 143). The first column shows the fluorescence of the membrane, the second the fluorescence of the

1 MamK filament and the third column is a superposition of the images of the two first columns. The
2 spatial distribution of MamK suggests that the filaments form clusters.

3

4 The data above show that the distribution of MamK is more complex than that previously
5 thought, and highlight the need for more detailed high-resolution imaging. However, it is
6 worth pointing out that our fluorescence microscopy data does not necessarily suggest that
7 the magnetosome filament is not straight, and it might simply be a consequence of the
8 dynamic localization of the proteins that finally assemble as bundles along the
9 magnetosome chain to provide the commonly accepted template for the mechanical
10 stabilization of the magnetosome chain.

11

12 **4. Conclusions**

13 In conclusion, we have seen that magnetotactic bacteria are able to produce magnetosomes
14 and align them in a chain that is nearly perfectly 1D. Further work will however be
15 necessary to determine the organization of the magnetosomes in 3D, in the case of the most
16 studied spirilla, but also for other bacterial morphology and as a function of magnetosome
17 organization since some strains produce more than one chain per bacterium. Cryo-FIB may
18 become a powerful tool to advance this problematic but will remain impeded by the time
19 consuming nature of current electron tomographic techniques.

20

21 In addition, if also the established MamJ/MamK system is very appealing because of its
22 simplicity and apparent widespread application, we recall here that the MamJ protein is not
23 universally conserved, but absent from many magnetotactic bacteria where chains are
24 observed. Therefore an alternative scenario must be considered. Furthermore, it was shown
25 that the phenotype associated with *mamK* deletion mutant in MSR-1 and AMB-1 is not fully
26 consistent with the presented model, since clusters of magnetosomes would be expected if

1 those would be free to move. This is a further hint towards a binding of the magnetosomes
2 not only to MamK filaments but also to another structure that can be the inner membrane
3 as shown in Figure 3 or another structure to be identified.

4

5 Here we also show that the MamK filaments are not only found next to the magnetosome
6 chain, but that its intracellular localization is much more dispersed than initially described /
7 thought, possibly partly due to reduced resolution associated with optical microscopic
8 techniques. This could be interpreted as a further indication that MamK is not only the
9 protein being at the origin of the materials building the magnetosome filament but might
10 also be involved in the directed transport of the magnetosomes as suggested by our
11 simulations and previous experimental work⁴⁴.

12 Still, we are convinced that the magnetotactic bacteria represent an interesting model for a
13 possible way of forming a functional magnetic anisotropic structure serving as actuator. Such
14 actuators are difficult to form synthetically but would be of interest for numerous
15 applications and therefore, there is still much to learn from these microorganisms, more
16 intricate than initially thought.

17

18 **Acknowledgements**

19 Preliminary experiments on super-resolution microscopy were realized in the School of
20 Physics at the University of Edinburgh in the Collaborative Optical Spectroscopy
21 Micromanipulation and Imaging Centre (COSMIC) and were supported by the European Soft
22 Matter Infrastructure through the grant E110900113. MB and AK are grateful to Dr Jochen
23 Arlt for managing their visit at COSMIC. DF acknowledges funding from the European
24 Research Council (Starting Grant MB2 n°256915) and the Max Planck Society.

25

26 **References**

- 1 1. M.-P. Pileni, *Nanocrystals forming mesoscopic structures*, Wiley - VCH,
2 Weinheim, 2005.
- 3 2. S. Mann, *Nat. Mater.*, 2009, **8**, 781-792.
- 4 3. D. J. Dunlop and O. Özdemir, *Rock magnetism: fundamentals and frontiers*,
5 Cambridge University Press, Cambridge, 1997.
- 6 4. M. Kumari, M. Widdrat, É. Tompa, R. Uebe, D. Schüler, M. Pósfai, D. Faivre
7 and A. M. Hirt, *J. Appl. Phys.*, 2014, **116**, 124304.
- 8 5. A. R. Muxworthy and W. Williams, *J. Geophys. Res.*, 2006, **111**, B12S12.
- 9 6. M. Widdrat, M. Kumari, É. Tompa, M. Pósfai, A. M. Hirt and D. Faivre,
10 *ChemPlusChem*, 2014, n/a-n/a.
- 11 7. A. R. Muxworthy and W. Williams, *J. R. Soc. Interface*, 2009, **6**, 1207-1212.
- 12 8. A. Ahniyaz, Y. Sakamoto and L. Bergström, *Proc. Natl. Acad. Sci. U.S.A.*,
13 2007, **104**, 17570-17574.
- 14 9. D. Faivre and D. Schüler, *Chem. Rev.*, 2008, **108**, 4875-4898.
- 15 10. Christopher T. Lefèvre, M. Bennet, L. Landau, P. Vach, D. Pignol, Dennis A.
16 Bazylinski, Richard B. Frankel, S. Klumpp and D. Faivre, *Biophys. J.*, 2014,
17 **107**, 527-538.
- 18 11. M. Bennet, A. McCarthy, D. Fix, M. R. Edwards, F. Repp, P. Vach, J. W. C.
19 Dunlop, M. Sitti, G. S. Buller, S. Klumpp and D. Faivre, *PLoS One*, 2014, **9**,
20 e101150.
- 21 12. A. Fischer, M. Schmitz, B. Aichmayer, P. Fratzl and D. Faivre, *J. R. Soc.*
22 *Interface*, 2011, **8**, 1011-1018.
- 23 13. A. Scheffel, A. Gärdes, K. Grünberg, G. Wanner and D. Schüler, *J. Bacteriol.*,
24 2008, **190**, 377-386.
- 25 14. D. Murat, V. Falahati, L. Bertinetti, R. Csencsits, A. Körnig, K. H. Downing,
26 D. Faivre and A. Komeili, *Mol. Microbiol.*, 2012, **85**, 684-699.
- 27 15. D. Murat, A. Quinlan, H. Vali and A. Komeili, *Proc. Natl. Acad. Sci. U.S.A.*,
28 2010, **107**, 5593-5598.
- 29 16. A. Lohße, S. Borg, O. Raschdorf, I. Kolinko, E. Tompa, M. Pósfai, D. Faivre, J.
30 Baumgartner and D. Schüler, *J. Bacteriol.*, 2014, **196**, 2658-2669.
- 31 17. A. Lohße, S. Ullrich, E. Katzmann, S. Borg, G. Wanner, M. Richter, B. Voigt,
32 T. Schweder and D. Schüler, *PLoS One*, 2011, **6**, e25561.
- 33 18. A. Arakaki, J. Webbs and T. Matsunaga, *J. Biol. Chem.*, 2003, **278**, 8745-
34 8750.
- 35 19. A. Körnig, M. Winklhofer, J. Baumgartner, T. P. Gonzalez, P. Fratzl and D.
36 Faivre, *Adv. Funct. Mater.*, 2014, **24**, 3926-3932.
- 37 20. D. Faivre, A. Fischer, I. Garcia-Rubio, G. Mastrogiacomo and A. U. Gehring,
38 *Biophys J.*, 2010, **99**, 1268-1273.
- 39 21. M. Charilaou, K. K. Sahu, D. Faivre, A. Fischer, I. García-Rubio and A. U.
40 Gehring, *Appl. Phys. Lett.*, 2011, **99**, 182504.
- 41 22. S. Klumpp and D. Faivre, *PLoS One*, 2012, **7**, e33562.
- 42 23. E. AlphanDéry, Y. Ding, A. T. Ngo, Z. L. Wang, L. F. Wu and M. P. Pileni, *ACS*
43 *Nano*, 2009, **3**, 1539-1547.
- 44 24. O. Draper, M. E. Byrne, Z. Li, S. Keyhani, J. C. Barrozo, G. Jensen and A.
45 Komeili, *Mol. Microbiol.*, 2011, **82**, 342-354.
- 46 25. E. Katzmann, A. Scheffel, M. Gruska, J. M. Plitzko and D. Schüler, *Mol.*
47 *Microbiol.*, 2010, **77**, 208-224.
- 48 26. A. Komeili, Z. Li, D. K. Newman and G. J. Jensen, *Science*, 2006, **311**, 242-
49 245.

- 1 27. A. Scheffel, M. Gruska, D. Faivre, A. Linaroudis, J. M. Pitzko and D. Schüler,
2 *Nature*, 2006, **440**, 110-115.
- 3 28. A. Scheffel and D. Schüler, *J. Bacteriol.*, 2007, **189**, 6437-6446.
- 4 29. M. A. Carillo, M. Bennet and D. Faivre, *J. Phys. Chem. B*, 2013, **117**, 14642-
5 14648.
- 6 30. N. Pradel, C.-L. Santini, A. Bernadac, Y. Fukumori and L.-F. Wu, *Proc. Natl.*
7 *Acad. Sci. U.S.A.*, 2006, **103**, 17485-17489.
- 8 31. E. Ozyamak, J. Kollman, D. A. Agard and A. Komeili, *J. Biol. Chem.*, 2013,
9 **288**, 4265-4277.
- 10 32. J. B. Rioux, N. Philippe, S. Pereira, D. Pignol, L. F. Wu and N. Ginet, *PLoS*
11 *One*, 2010, **5**, 12.
- 12 33. S. Sonkaria, G. Fuentes, C. Verma, R. Narang, V. Khare, A. Fischer and D.
13 Faivre, *PLoS One*, 2012, **7**, e34189.
- 14 34. A. Taoka, R. Asada, L. F. Wu and Y. Fukumori, *J. Bacteriol.*, 2007, **189**,
15 8737-8740.
- 16 35. A. Körnig, J. Dong, M. Bennet, M. Widdrat, J. Andert, F. D. Müller, D. Schüler,
17 S. Klumpp and D. Faivre, *Nano Lett.*, 2014, **14**, 4653-4659.
- 18 36. K. He, J. Sun and X. Tang, *Ieee Trans. Pattern Anal. Mach. Intell.*, 2013, **35**,
19 1397-1409.
- 20 37. E. Betzig, G. H. Patterson, R. Sougrat, O. W. Lindwasser, S. Olenych, J. S.
21 Bonifacino, M. W. Davidson, J. Lippincott-Schwartz and H. F. Hess, *Science*,
22 2006, **313**, 1642-1645.
- 23 38. P. Dedecker, S. Duwe, R. K. Neely and J. Zhang, *Journal of Biomedical Optics*,
24 2012, **17**.
- 25 39. D. Faivre, L. H. Böttger, B. F. Matzanke and D. Schüler, *Angew. Chem. Int.*
26 *Ed.*, 2007, **46**, 8495-8499.
- 27 40. S. S. Kalirai, D. A. Bazylnski and A. P. Hitchcock, *PLoS One*, 2013, **8**,
28 e53368.
- 29 41. M. B. Elowitz, M. G. Surette, P. E. Wolf, J. B. Stock and S. Leibler, *J. Bacteriol.*,
30 1999, **181**, 197-203.
- 31 42. M. Kumar, M. S. Mommer and V. Sourjik, *Biophys. J.*, 2010, **98**, 552-559.
- 32 43. S. Klumpp and R. Lipowsky, *Phys. Rev. Lett.*, 2005, **95**, 268102.
- 33 44. E. Katzmann, F. D. Müller, C. Lang, M. Messerer, M. Winklhofer, J. M. Pitzko
34 and D. Schüler, *Mol. Microbiol.*, 2011, **82**, 1316-1329.
- 35 45. F. Popp, J. P. Armitage and D. Schüler, *Nat. Commun.*, 2014, **5**.
- 36
37